Quantum Science and Technology

PAPER • **OPEN ACCESS**

A many-body heat engine at criticality

To cite this article: Thomás Fogarty and Thomas Busch 2021 *Quantum Sci. Technol.* **6** 015003

Quantum Science and Technology

OPEN ACCESS

RECEIVED
20 July 2020

REVISED
28 September 2020

ACCEPTED FOR PUBLICATION
28 September 2020

PUBLISHED
6 November 2020

PAPER

A many-body heat engine at criticality

Thomás Fogarty* and **Thomas Busch**

Quantum Systems Unit, Okinawa Institute of Science and Technology Graduate University, Onna, Okinawa 904-0495, Japan

* Author to whom any correspondence should be addressed.

E-mail: thomas.fogarty@oist.jp

Keywords: quantum thermodynamics, ultracold atoms, quantum criticality, Tonks-Girardeau gas, shortcuts to adiabaticity

Supplementary material for this article is available online

Abstract

We show that a quantum Otto cycle in which the medium, an interacting ultracold gas, is driven between a superfluid and an insulating phase can outperform similar single particle cycles. The presence of an energy gap between the two phases can be used to improve performance, while the interplay between lattice forces and the particle distribution can lead to a many-body cooperative effect. Since finite time driving of this cycle can create unwanted non-equilibrium dynamics which can significantly impair the performance of the engine cycle, we also design an approximate shortcut to adiabaticity for the many-body state that can be used to achieve an efficient Otto cycle around a critical point.

1. Introduction

The almost unmatched precision of controlling and measuring cold atomic systems provided by recent experiments has made them forerunners in the area of quantum simulations [1–3]. In particular their many-body aspect and the ability to create out-of-equilibrium situations in a controlled way has led to paradigmatic results that are beyond even advanced numerical simulations [4]. They therefore offer an exciting testbed for exploring ideas in quantum thermodynamics [5], ranging from insights into the understanding of work and heat at the quantum level to the operation of quantum heat engines (QHE) and refrigerators [6–11]. Describing such machines taking fundamental quantum effects into account has already led to a number of unexpected results and can allow one to achieve certain advantages over comparable classical systems. In recent years this has been shown for machines operating across quantum phase transitions [12–18], using squeezed baths as quantum environments [19–23], or exploiting the cooperative effects of many-body quantum systems [24–31].

However, the description of interacting many-particle systems at finite temperatures is a non-trivial problem and solvable models only exist in restricted circumstances that are often not experimentally realistic. One notable exception to this are the recently realised Tonks–Girardeau (TG) gases of strongly interacting bosons in effectively one-dimensional settings [32, 33], where exact solutions can be found using the Bose–Fermi mapping theorem at finite temperatures [34–37]. Therefore they lend themselves to exact studies of thermodynamical machines.

In this work we consider a TG gas in a box and realise the compression and expansion strokes a heat engine requires by the switching on and off of an optical lattice potential. This changes the one-dimensional volume the system has available and also leads to significant changes in the energy spectrum. Moreover, in such a system the particle filling statistics plays an important role, as at low temperature and unit filling an insulating phase forms as soon as an infinitesimally weak lattice potential is applied [38, 39]. This phase transition is called the pinning-transition and it is signalled by the appearance of an energy gap in the spectrum. One can therefore drive a quantum Otto cycle between the superfluid and insulating phases by simply switching the lattice on and off. As the operation of the engine cycle is dependent on the energy spectrum of the particles, the presence of the energy gap at the quantum critical point can drastically change the engine performance. Furthermore, due to the competing influence of the lattice potential

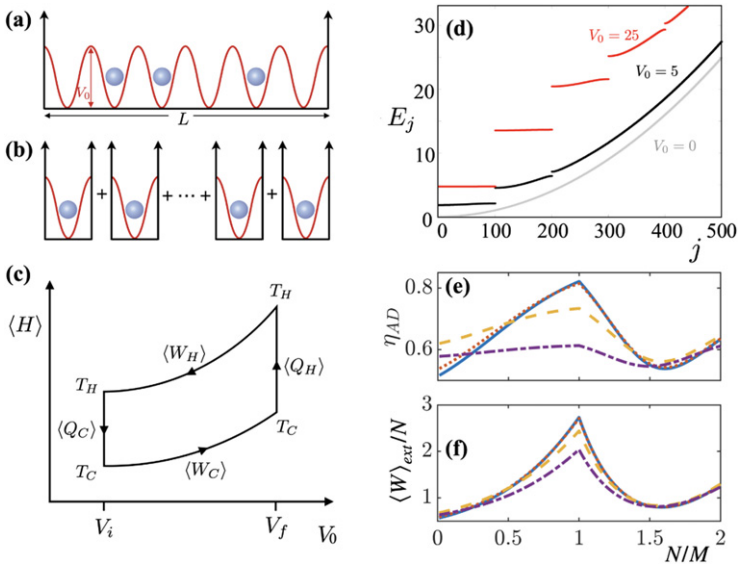

Figure 1. (a) Schematic of the setup for the mQHE and (b) the sQHE. (c) Schematic of the Otto cycle. (d) Single particle spectrum E_j of a lattice with $M = 100$ wells and $V_0 = 0$ (light grey), $V_0 = 5$ (black) and $V_0 = 25$ (red). (e) Efficiency and (f) work output for an adiabatic cycle as a function of the filling ratio N/M, with $T_C = 0$, $T_H = 5$ and $V_f = 50$. Different values of V_i are shown, $V_i = 0$ (blue solid), $V_i = 1$ (red dotted), $V_i = 5$ (yellow dashed) and $V_i = 10$ (purple dot-dashed). The work output is scaled with the number of particles N.

and the particle interactions, nontrivial energy spectra can be achieved that may exhibit a many-body cooperative effect on the engine cycle. This can be quantified by comparing the many-body quantum heat engine (mQHE) with an equivalently sized ensemble of non-interacting single particle quantum heat engines (sQHE) [27].

Of course, any realistic implementation of a QHE cycle must be carried out on a finite timescale, which can have a negative impact on the resulting engine performance. If the cycle is performed too quickly, the excitation of non-equilibrium states may act as a form of inner friction due to the irreversible nature of the dynamics, thereby reducing performance [40, 41]. While adiabatic dynamics preserve the reversibility of the cycle through the slow driving of the quantum state, the long timescales required result in negligible output power. To achieve both, engine cycles that are efficient and fast, one can employ the techniques of shortcuts to adiabaticity (STA), which allow for adiabatic dynamics on finite timescales [8, 28, 42–49]. However, since the driven dynamics of our interacting many-particle system encompasses the quantum critical point at the pinning transition, standard STA approaches cannot be easily employed. We therefore derive and implement a many-body STA using a variational approach [50, 51], which, although approximate in nature, improves the performance of the engine when compared to a non-optimised cycle.

2. Methods

The system we consider consists of a gas of N particles of mass m which are trapped in an effectively one dimensional box potential, $V_B(x)$, of length L with infinitely high walls. The single particle Hamiltonian is given by

$$H = -\frac{\hbar^2}{2m}\nabla^2 + V_B(x) + V_l(x,t), \tag{1}$$

where we have also included a time-dependent optical lattice potential of the form $V_l(x,t) = V_0(t)\cos^2(k_0 x + \phi)$ (see figure 1(a)). The lattice vector is given by $k_0 = M\pi/L$ and M is the number of wells. We choose $\phi = 0$ for M even and $\phi = \pi/2$ for M odd to ensure that there are no half lattice sites at the edge of the box. We also choose to fix k_0 and scale the size of the box potential to change the number of lattice sites.

The eigenstates, $\psi_n(x)$ (which we calculate through exact diagonalization), of the Hamiltonian (1) can be used to describe a gas of spinless fermions via the Slater determinant $\Psi_F(x_1, x_2, \ldots, x_N) = \frac{1}{\sqrt{N!}}\det_{n,j=1}^{N}[\psi_n(x_j)]$, which can be mapped onto a TG gas of hard-core bosons after appropriate symmetrization as $\Psi_B(x_1, x_2, \ldots, x_N) = \prod_{1\leqslant i<j\leqslant N}\mathrm{sgn}(x_i - x_j)\Psi_F(x_1, x_2, \ldots, x_N)$ [34, 52]. This duality can be understood by realising that the spatial distribution of the fermions is governed by a pseudo-interaction implied by the Pauli exclusion principle (Fermi pressure), which has the same effect as

the strongly repulsive interaction present in the TG gas. Their respective densities are therefore trivially identical, and this equivalence also extends to their thermodynamic behaviours which are governed by the Fermi–Dirac occupation factors, $f_n = [e^{(E_n-\mu)/k_BT}+1]^{-1}$ (with E_n the eigenenergies, μ the chemical potential and k_B the Boltzmann constant) [35, 37, 53]. This implies that the engine cycles will be identical as well. In the following we will scale all energies in units of the lattice recoil energy, $E_R = \hbar^2k_0^2/(2m)$, and temperature in units of E_R/k_B.

We consider a quantum Otto cycle (see figure 1(c)) driven between two lattice depths, $V_0 = \{V_i, V_f\}$, at different lattice filling ratios, N/M. The cycle consists of four strokes: (i) isentropic *compression* (lattice raising from depth V_i to V_f) over a time t_1 at fixed temperature T_C; (ii) weak coupling to a thermal bath at temperature $T_H > T_C$ during a time t_2; (iii) isentropic *expansion* (lattice lowering from depth V_f to V_i) over a time t_3; and (iv) weak coupling to a thermal bath at temperature T_C for a time t_4. During the isentropic compression and expansion strokes we assume the system is isolated from the respective thermal reservoirs.

We consider a reversible cycle where the dynamics of the quantum state are sufficiently slow so as to be considered adiabatic (denoted by the subscript AD). The work done during the isentropic strokes can be calculated from the difference in energy between the many-body states at lattice depths V_i and V_f at the different temperatures, $\langle W_C\rangle = \langle H_{T_C}(V_f)\rangle - \langle H_{T_C}(V_i)\rangle$ and $\langle W_H\rangle = \langle H_{T_H}(V_i)\rangle - \langle H_{T_H}(V_f)\rangle$, with $\langle H\rangle = \mathrm{Tr}(H\rho)$ being the expectation value of the energy of the thermal states. The heat exchanged with the cold and hot baths is the given by $\langle Q_C\rangle = \langle H_{T_C}(V_i)\rangle - \langle H_{T_H}(V_i)\rangle$ and $\langle Q_H\rangle = \langle H_{T_H}(V_f)\rangle - \langle H_{T_C}(V_f)\rangle$ and the efficiency and output power can be calculated as

$$\eta_{AD} = -\frac{\langle W_C\rangle + \langle W_H\rangle}{\langle Q_H\rangle}, \qquad P_{AD} = -\frac{\langle W_C\rangle + \langle W_H\rangle}{\tau}, \tag{2}$$

where $\langle W\rangle_{ext} = -\left(\langle W_C\rangle + \langle W_H\rangle\right)$ is the work output and $\tau = t_1 + t_2 + t_3 + t_4$ is the duration of the cycle.

3. Results

3.1. Adiabatic cycle

For the performance of the engine the filling fraction N/M plays an important role. At $T_C = 0$ and for an incommensurate filling, $N \neq M$, the particles are delocalized in the lattice and can move within the box. However, for a commensurate filling, $N = M$, a pinning transition occurs for any infinitesimal lattice strength, whereby each particle becomes more strongly localized at an individual lattice site, which significantly restricts its motion [54, 55]. The behaviour of this insulating phase is then determined by the energy gap in the single particle spectrum (see figure 1(d)) which has a size of approximately $V_0/2$ for shallow lattices and $2\sqrt{V_0}$ for deep lattices [38]. The differences in the accessible single particle excitation spectrum for N/M therefore lead to different behaviours when running the engine and in figures 1(e) and (f) one can clearly see that peak performance is achieved at unit filling. At this point the particles in the cold adiabat fill the lowest energy band and as V_0 is increased the energy gap is widened. Thermal excitations induced by the hot bath then allow particles to jump the gap and therefore more energy can be extracted as the lattice depth is decreased along the hot adiabat. As the high performance regime is the interesting one for heat engines, we will focus on the case of unit filling in the following.

The advantage of exploiting the critical point in a mQHE with N particles can be quantified by comparison with an ensemble of N sQHE, see figure 1(b). Each sQHE obeys the Hamiltonian given by equation (1) with a box length of $L = \pi/k_0$, so that exactly one lattice well is present, $V_l = V_0\cos(k_0x + \pi/2)$. The Otto cycle is then carried out using the same lattice height and bath temperatures, however in the mQHE the final state is strongly influenced by the presence of the interparticle interactions and the periodicity of the optical lattice. To quantify the difference between the mQHE and the sQHE, we calculate the ratio of their respective efficiencies and powers

$$\eta^*(N) = \frac{\eta(N)}{\eta(1)}, \qquad P^*(N) = \frac{P(N)}{NP(1)}, \tag{3}$$

such that $\eta^*(N) > 1$ and $P^*(N) > 1$ indicate that the many-body state gives a performance boost [27].

In figure 2(a) we show the efficiency ratio for an adiabatic cycle as a function of the lattice depths V_i and V_f. For $V_f > V_i$ the cycle produces positive work and therefore acts as an engine. One can see that large many-body cooperative effects can be achieved in the regime where both lattices are weak, and where therefore the particles in the mQHE are still partially overlapping. This results in a non-trivial, non-flat single-particle energy spectrum (see figure 1(d)) and therefore in enhanced efficiency and power output over the sQHE. When both lattices are deep, $V_0 \gtrsim 30$, the particles are highly localized in individual lattice sites and the single particle energy spectrum becomes degenerate forming flat bands. In this limit all

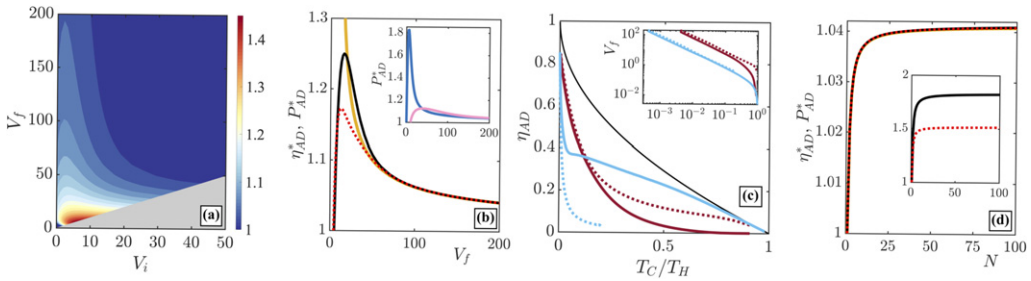

Figure 2. (a) Efficiency ratio $\eta^*_{\rm AD}$ as a function of the initial lattice depth V_i and the final lattice depth V_f. The system is at unit filling with $N = M = 100$, while the temperatures of the cold and hot reservoirs are $T_{\rm C} = 0$ and $T_{\rm H} = 5$, respectively. The grey region indicates the parameter space where $V_i > V_f$, in which no work can be extracted from the cycle. (b) Numerical values for $\eta^*_{\rm AD}$ (red dotted line) and $P^*_{\rm AD}$ (black solid line) compared to the approximation given in equation (4) (yellow solid line) as function of V_f for $T_{\rm H} = 5$ with $N = M = 100$. The inset shows $P^*_{\rm AD}$ for $T_{\rm H} = 1$ (blue line) and $T_{\rm H} = 20$ (pink line). (c) Efficiency at maximum power (see text) and shown as a function of $T_{\rm C}/T_{\rm H}$ for two temperatures of the cold adiabat: $T_{\rm C} = 0.01$ (light blue lines) and $T_{\rm C} = 0.1$ (dark red lines). The solid lines are for the mQHE, the dotted ones for the sQHE and the black line indicates the Curzon–Ahlborn limit. The inset shows the values of V_f which correspond to the maximum power for each respective cycle (in log–log scale as a function of $T_{\rm C}/T_{\rm H}$). (d) Dependence of $\eta^*_{\rm AD}$ (red dotted line) and $P^*_{\rm AD}$ (black solid line) as a function of N at unit filling with $T_{\rm H} = 5$ and with $V_f = 200$. The numerical results are indistinguishable from equation (4). The inset shows $\eta^*_{\rm AD}$ and $P^*_{\rm AD}$ for $T_{\rm H} = 1$ and $V_f = 5$.

many-body cooperative effects are lost and the mQHE becomes equivalent to the sQHE. Since for weak initial lattice depths, $V_i \lesssim 10$, the mQHE shows enhanced performance for a range of values of V_f, we will focus on this region of the parameter space in what follows, specifically considering the limiting case of initially having free particles ($V_i \to 0$).

Indeed, for mQHE cycles which operate at low reservoir temperatures, $\theta = \frac{E_{\rm R}}{k_{\rm B} T_{\rm H}} \sqrt{V_f} > 1$, and which ramp to deep lattices, $V_f \gg 1$, it is possible to find an approximate expression for the many-body performance boost,

$$\eta^*_{\rm AD}(N) = P^*_{\rm AD}(N) \approx 1 + \frac{1 - 1/N}{\Delta - \frac{3}{2}\left[\coth(\theta) + 1\right]}, \tag{4}$$

where $\Delta = 2\sqrt{V_f} - 1$ is the energy gap (see Supplemental Material for details). From this one can immediately see that at unit filling the mQHE will always outperform the sQHE once $V_f > 4$. Furthermore, increasing the number of particles and reaching the state of double filling, $N = 2M$, where the two lowest states of each lattice site are occupied, does not lead to improved performance. In the limits $\theta, M \to \infty$ the efficiency ratio can be written as $\eta^*(2M) \equiv \frac{\eta(2M)}{\eta(1)} \to \frac{1-4(\Delta-1)^{-1}}{1-3\Delta^{-1}}$, showing that for $V_f > 1$ the efficiency of the sQHE is always larger than the mQHE at double filling, which is due to the anharmonicity of the individual lattice sites leading to reduced gaps between higher lying energy states.

In figure 2(b) we show the numerically obtained values of the ratios $\eta^*_{\rm AD}(N)$ and $P^*_{\rm AD}(N)$ as a function of V_f in comparison to the approximation in equation (4). One can see that the exact ratios peak at lower values of V_f, which is due to the fact that the particles in the many-body state are still partially delocalized and therefore many-body cooperativity is stronger. For deeper lattices, $V_f \gtrsim 50$, both ratios head towards one, as stronger localisation makes the lattice sites become effectively independent. The decay of the many-body advantage is well described by the approximation in equation (4) (solid yellow line in figure 2(b)) and given by a $1/\Delta$ dependence. While the decay is universal, the position and height of the maximum depend on the other parameters of the system, in particular $T_{\rm H}$ (see inset of figure 2(b)). In general, a significant many-body advantage exists by operating the mQHE in weak lattices and at low temperatures when the commensurate system remains close to the quantum critical point. At higher temperatures the existing thermal energies diminish the importance of the energy gap and the quantum criticality is washed out. To demonstrate this we show in figure 2(c) the efficiency at maximum power (optimised over the lattice depth V_f, see inset in figure 2(c)) for two different temperatures of the cold adiabat: one deep in the quantum regime $T_{\rm C} = 0.01$, which ensures that the system is in its ground state and therefore close to the quantum critical point; the other at a slightly higher temperature $T_{\rm C} = 0.1$, where the effect of the quantum criticality is reduced. When $T_{\rm H}$ is small, the mQHE with the lower $T_{\rm C}$ can be seen to be more efficient and close to the Curzon–Ahlborn efficiency, $\eta_{\rm CA} = 1 - \sqrt{T_{\rm C}/T_{\rm H}}$, which is a good indicator of the performance of the Otto cycle [29, 46, 56]. Furthermore, it is worth noticing that at higher $T_{\rm C}$ the mQHE is outperformed by the sQHE as the thermal energy leads to less localisation within the box potential and the energy gap is washed out. Therefore, this quantum critical mQHE only shows enhanced performance at low temperatures when the system is close to the critical point.

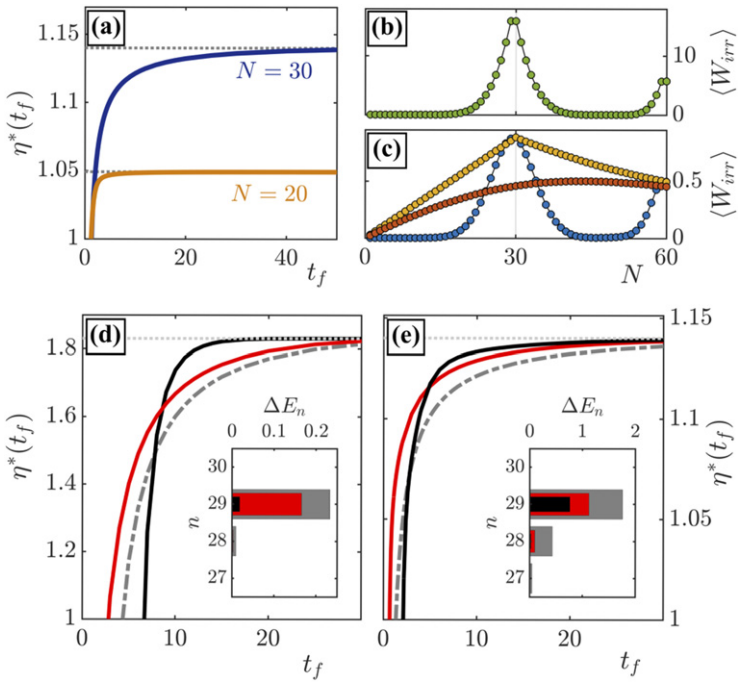

Figure 3. (a) Efficiency ratio η^* as a function of ramp time t_f for $M = 30$ with $V_f = 25$ and $T_H = 5$ (P^* behaves similarly and is not shown) at the pinning transition point ($N = 30$) and away from it ($N = 20$). (b and c) Irreversible work created during a process with a ramp time of $t_f = 2$ as a function of total particle number N. (b) $\langle W_{irr}\rangle$ for ramping on the lattice at $T_C = 0$, (c) $\langle W_{irr}\rangle$ for ramping off the lattice at $T_H = 0$ (blue), $T_H = 0.5$ (yellow) and $T_H = 5$ (red). Efficiency ratio for (d) $V_f = 5$ and $T_H = 0.5$ and (e) $V_f = 25$ and $T_H = 5$ after implementing the non-optimised ramp $V_\lambda(t)$ (grey dot dashed), and the STAs $\langle V^{STA}(t)\rangle$ (red) and $V^{STA}_{M-1}(t)$ (black). Insets: energy difference between the non-adiabatic and adiabatic single particle energies after each ramp, $\Delta E_n = E_n^{NA} - E_n^{AD}$, taking $t_f = 15$ and with the colour code matching that of the larger panels.

In deep lattices the power and efficiency ratios are equivalent for any number of lattice sites at unit filling ($N = M$) and they are exactly described by equation (4) (see figure 2(d)). As the many-body advantage is proportional to $(1 - 1/N)$, one can see a rapid increase in both quantities for increasing particle number until $N \sim 10$, after which it asymptotically approaches $1 + (\Delta - 3)^{-1}$ in the thermodynamic limit. In more shallow lattices the efficiency and power ratios asymptotically reach different, but overall larger values, while the dependence on N remains consistent with the behaviour observed for deep lattices (see inset of figure 2(d)). Indeed, one does not need to create large many-body states to see a marked improvement in engine performance, rather only a few dozen particles are sufficient for observing the effects of many-body cooperativity in this system.

3.2. Finite time cycle

While all the results above are obtained for a reversible cycle which undergoes adiabatic dynamics, this results in negligible power output due to the long timescales for each cycle, therefore necessitating fast engine cycles for finite power-output. However, fast driving through a critical point will inevitably result in non-adiabatic dynamics and irreversible work being produced, with the latter being defined as the difference between the average work of the non-adiabatic (NA) and adiabatic driving, $\langle W_{irr}\rangle = \langle W\rangle_{NA} - \langle W\rangle_{AD}$. This ultimately leads to reduced performance of the QHE [57–59]. To explore the effect of irreversible work on the engine performance we numerically calculate the unitary dynamics of the single particle states during the compression and expansion strokes, $\psi_n(x,t) = e^{-\frac{i}{\hbar}\int_0^t H(t')dt'}\psi_n(x,0)$, describing the insertion and removal of the optical lattice over a finite time t_f (in units of $2\pi/E_R$). We parametrise the lattice strength as $V_\lambda(t) = \lambda(t)V_f\cos^2(k_0x)$, with $\lambda(t) = t^3/t_f^3[1 + 3(1 - t/t_f) + 6(1 - t/t_f)^2]$, which is sufficient to explore the dynamical properties of a finite time engine stroke, but is not necessarily optimal for the system [60–63]. As our focus is on the non-adiabatic dynamics initiated by the lattice ramp we will neglect the dynamics during the coupling to the different heat baths and assume that the thermalization times t_2 and t_4 are much shorter than the times for the work strokes t_1 and t_3 [42, 64]. Taking $t_1 = t_3 \equiv t_f$, the total time for the cycle is $\tau \approx 2t_f$.

For a finite time cycle at commensurate filling the efficiency only slowly approaches the adiabatic efficiency (see figure 3(a)) due to the large amount of irreversible work created when driving the system at the pinning transition (see figures 3(b) and (c)). In comparison, incommensurate fillings produce

significantly less irreversible work as excitations are far from the energy gap and therefore the adiabatic efficiency can be reached for significantly shorter ramp times. Also note that more irreversibility is created during the raising of the barrier compared to the lowering, as the opening of the energy gap adds to the nonequilibrium excitations.

Even with the advantage gained from the energy gap, the resulting irreversible dynamics on short timescales set a limit on the performance of the engine cycle. In fact, this problem does not just appear in dynamics about a critical point, but is present in any non-adiabatic driving of QHE. To improve engine performance on finite timescales different STA approaches have been suggested [28, 42, 43, 46, 65–67]. However, while STAs have been successfully developed for non-interacting and mean-field systems, designing them for strongly interacting many-body systems poses new challenges when scale invariance can not be exploited [50], and is especially difficult due to the orthogonality catastrophe in larger systems [48, 68]. We therefore employ a variational approach which can find the optimal driving amplitude $V_n^{\mathrm{STA}}(t)$ for each of the single particle functions $\psi_n(x,t)$ which are used in the Slater determinant to construct the many-body state [51]. However, while this in principle can optimise the dynamics of each $\psi_n(x,t)$ individually, in practice a single lattice ramp must act on the entire many-body state and the chosen $V_n^{\mathrm{STA}}(t)$ may create unwanted excitations in different $\psi_m(x,t)$, for $m \neq n$.

We therefore consider two different approximate STAs to optimize the many-body dynamics. First, we choose the average of the STA pulses for all states up to the energy gap, $\langle V^{\mathrm{STA}}(t)\rangle = \sum_{n=1}^{M} V_n^{\mathrm{STA}}(t)/M$, and numerically time evolve the single particle states with this finite time ramp. While this shows an improvement over the non-optimized ramp $V_\lambda(t)$ for all timescales (see figures 3(d) and (e)), it is only marginal as the optimization is averaged over the whole system. We therefore also consider the ramp $V_{M-1}^{\mathrm{STA}}(t)$, which specifically optimizes the most irreversible single particle state, $\psi_{M-1}(x)$, which sits just below the gap and possesses the most excess energy after the V_λ ramp (see insets in figures 3(d) and (e)). This STA results in a larger efficiency gain as excitations of this state are mostly suppressed, and the adiabatic limit is quickly reached when the lattice is weak. However, this STA becomes ineffective for fast cycles, as large modulations in the approximate STA ramp can induce excitations in the rest of the system, which is a limitation of using these approximate techniques to design STAs for many-body states.

4. Conclusions

In summary, we have described the operation of a quantum Otto cycle about a critical point in a strongly interacting many-particle system. We have shown that such a setup can yield increased performance due to the presence of an energy gap and cooperative many-body effects which arise due to competition between interactions and lattice forces. Using the particular cold-atom setup we have chosen, which has already been experimentally studied [39], clearly highlights the dynamical effects stemming from the ordering when going through the critical point and the complex dynamics that arises during non-trivial shortcut driving. Furthermore, recent experiments have shown that many-particle heat engines can be realized with two-component ultracold gases [69], whereby inelastic spin-exchange collisions are used to transfer heat between the engine and the bath. Accordingly, our work lays foundations for the further exploration of STA techniques for interacting many-body systems and their potential applications in QHE.

Acknowledgments

We thank Blaithín Power, John Goold and Steve Campbell for efficient discussions. This work was supported by the Okinawa Institute of Science and Technology Graduate University and JSPS KAKENHI-18K13507.

ORCID iDs

Thomás Fogarty https://orcid.org/0000-0003-4940-5861

References

[1] Lewenstein M, Sanpera A, Ahufinger V, Damski B, Sen(De) A and Sen U 2007 *Adv. Phys.* **56** 243–379
[2] Bloch I, Dalibard J and Nascimbène S 2012 *Nat. Phys.* **8** 267–76
[3] Gross C and Bloch I 2017 *Science* **357** 995–1001
[4] Polkovnikov A, Sengupta K, Silva A and Vengalattore M 2011 *Rev. Mod. Phys.* **83** 863–83
[5] Deffner S and Campbell S 2019 *Quantum Thermodynamics* vol 2053-2571 (San Rafael, CA: Morgan & Claypool Publishers)
[6] Kosloff R 1984 *J. Chem. Phys.* **80** 1625–31

[7] Fialko O and Hallwood D W 2012 *Phys. Rev. Lett.* **108** 085303
[8] Abah O, Roßnagel J, Jacob G, Deffner S, Schmidt-Kaler F, Singer K and Lutz E 2012 *Phys. Rev. Lett.* **109** 203006
[9] Roßnagel J, Dawkins S T, Tolazzi K N, Abah O, Lutz E, Schmidt-Kaler F and Singer K 2016 *Science* **352** 325–9
[10] Kosloff R and Rezek Y 2017 *Entropy* **19** 136
[11] Chen Y Y, Watanabe G, Yu Y C, Guan X W and del Campo A 2019 *npj Quant. Inf.* **5** 88
[12] Campisi M and Fazio R 2016 *Nat. Commun.* **7** 11895
[13] Fusco L, Paternostro M and De Chiara G 2016 *Phys. Rev.* E **94** 052122
[14] Fadaie M, Yunt E and Müstecaplıoğlu O E 2018 *Phys. Rev.* E **98** 052124
[15] Ma Y H, Su S H and Sun C P 2017 *Phys. Rev.* E **96** 022143
[16] Chand S and Biswas A 2018 *Phys. Rev.* E **98** 052147
[17] S R B , Mukherjee V, Divakaran U and del Campo A 2020 Universal finite-time thermodynamics of many-body quantum machines from kibble–zurek scaling (arXiv:2003.06607)
[18] Abiuso P and Perarnau-Llobet M 2020 *Phys. Rev. Lett.* **124** 110606
[19] Roßnagel J, Abah O, Schmidt-Kaler F, Singer K and Lutz E 2014 *Phys. Rev. Lett.* **112** 030602
[20] Niedenzu W, Gelbwaser-Klimovsky D, Kofman A G and Kurizki G 2016 *New J. Phys.* **18** 083012
[21] Manzano G, Galve F, Zambrini R and Parrondo J M R 2016 *Phys. Rev.* E **93** 052120
[22] Klaers J, Faelt S, Imamoglu A and Togan E 2017 *Phys. Rev.* X **7** 031044
[23] Niedenzu W, Mukherjee V, Ghosh A, Kofman A G and Kurizki G 2018 *Nat. Commun.* **9** 165
[24] Uzdin R 2016 *Phys. Rev. Appl.* **6** 024004
[25] Campaioli F, Pollock F A, Binder F C, Céleri L, Goold J, Vinjanampathy S and Modi K 2017 *Phys. Rev. Lett.* **118** 150601
[26] Vroylandt H, Esposito M and Verley G 2017 *Europhys. Lett.* **120** 30009
[27] Jaramillo J, Beau M and del Campo A 2016 *New J. Phys.* **18** 075019
[28] Beau M, Jaramillo J and del Campo A 2016 *Entropy* **18** 168
[29] Deffner S 2018 *Entropy* **20** 875
[30] Niedenzu W and Kurizki G 2018 *New J. Phys.* **20** 113038
[31] Ferraro D, Campisi M, Andolina G M, Pellegrini V and Polini M 2018 *Phys. Rev. Lett.* **120** 117702
[32] Paredes B, Widera A, Murg V, Mandel O, Fölling S, Cirac I, Shlyapnikov G V, Hänsch T W and Bloch I 2004 *Nature* **429** 277–81
[33] Kinoshita T, Wenger T and Weiss D S 2004 *Science* **305** 1125–8
[34] Girardeau M 1960 *J. Math. Phys.* **1** 516–23
[35] Lenard A 1966 *J. Math. Phys.* **7** 1268–72
[36] Vignolo P and Minguzzi A 2013 *Phys. Rev. Lett.* **110** 020403
[37] Atas Y Y, Bouchoule I, Gangardt D M and Kheruntsyan K V 2017 *Phys. Rev.* A **96** 041605
[38] Büchler H P, Blatter G and Zwerger W 2003 *Phys. Rev. Lett.* **90** 130401
[39] Haller E, Hart R, Mark M J, Danzl J G, Reichsöllner L, Gustavsson M, Dalmonte M, Pupillo G and Nägerl H C 2010 *Nature* **466** 597–600
[40] García-March M A, Fogarty T, Campbell S, Busch T and Paternostro M 2016 *New J. Phys.* **18** 103035
[41] Fusco L, Pigeon S, Apollaro T J G, Xuereb A, Mazzola L, Campisi M, Ferraro A, Paternostro M and De Chiara G 2014 *Phys. Rev.* X **4** 031029
[42] del Campo A, Goold J and Paternostro M 2014 *Sci. Rep.* **4** 6208
[43] Abah O and Lutz E 2018 *Phys. Rev.* E **98** 032121
[44] Deffner S, Jarzynski C and del Campo A 2014 *Phys. Rev.* X **4** 021013
[45] Zheng Y, Campbell S, De Chiara G and Poletti D 2016 *Phys. Rev.* A **94** 042132
[46] Abah O and Paternostro M 2019 *Phys. Rev.* E **99** 022110
[47] Martínez-Garaot S, Palmero M, Muga J G and Guéry-Odelin D 2016 *Phys. Rev.* A **94** 063418
[48] Sels D and Polkovnikov A 2017 *Proc. Natl Acad. Sci.* **114** E3909–16
[49] Abah O, Puebla R, Kiely A, Chiara G D, Paternostro M and Campbell S 2019 *New J. Phys.* **21** 103048
[50] Fogarty T, Ruks L, Li J and Busch T 2019 *SciPost Phys.* **6** 21
[51] Xu T N, Li J, Busch T, Chen X and Fogarty T 2020 *Phys. Rev. Res.* **2** 023125
[52] Girardeau M D and Wright E M 2000 *Phys. Rev. Lett.* **84** 5239–42
[53] Atas Y Y, Gangardt D M, Bouchoule I and Kheruntsyan K V 2017 *Phys. Rev.* A **95** 043622
[54] Lelas K, Ševa T, Buljan H and Goold J 2012 *Phys. Rev.* A **86** 033620
[55] Mikkelsen M, Fogarty T and Busch T 2018 *New J. Phys.* **20** 113011
[56] Curzon F L and Ahlborn B 1975 *Am. J. Phys.* **43** 22–4
[57] Campbell S 2016 *Phys. Rev.* B **94** 184403
[58] Hoang D T, Prasanna Venkatesh B, Han S, Jo J, Watanabe G and Choi M S 2016 *Sci. Rep.* **6** 27603
[59] Deffner S 2017 *Phys. Rev.* E **96** 052125
[60] Gericke T, Gerbier F, Widera A, Fölling S, Mandel O and Bloch I 2007 *J. Mod. Opt.* **54** 735–43
[61] Masuda S, Nakamura K and del Campo A 2014 *Phys. Rev. Lett.* **113** 063003
[62] Dolfi M, Kantian A, Bauer B and Troyer M 2015 *Phys. Rev.* A **91** 033407
[63] Zhou X, Jin S and Schmiedmayer J 2018 *New J. Phys.* **20** 055005
[64] Abah O and Lutz E 2017 *Europhys. Lett.* **118** 40005
[65] del Campo A, Rams M M and Zurek W H 2012 *Phys. Rev. Lett.* **109** 115703
[66] Li J, Fogarty T, Campbell S, Chen X and Busch T 2018 *New J. Phys.* **20** 015005
[67] Hartmann A, Mukherjee V, Niedenzu W and Lechner W 2020 *Phys. Rev. Res.* **2** 023145
[68] Fogarty T, Deffner S, Busch T and Campbell S 2020 *Phys. Rev. Lett.* **124** 110601
[69] Bouton Q, Nettersheim J, Burgardt S, Adam D, Lutz E and Widera A 2020 An endoreversible quantum heat engine driven by atomic collisions (arXiv:2009.10946)